

Imaging correlated wave functions of few-electron quantum dots: Theory and scanning tunneling spectroscopy experiments

Massimo Rontani* and Elisa Molinari

*CNR-INFM National Research Center S3 and Dipartimento di Fisica,
Università degli Studi di Modena e Reggio Emilia, Via Campi 213/A, 41100 Modena, Italy*

Giuseppe Maruccio,[†] Martin Janson, Andreas Schramm, Christian Meyer,

Tomohiro Matsui, Christian Heyn, Wolfgang Hansen, and Roland Wiesendanger
Institute of Applied Physics, University of Hamburg, Jungiusstrasse 11 20355 Hamburg, Germany

(Dated: February 5, 2008)

We show both theoretically and experimentally that scanning tunneling spectroscopy (STS) images of semiconductor quantum dots may display clear signatures of electron-electron correlation. We apply many-body tunneling theory to a realistic model which fully takes into account correlation effects and dot anisotropy. Comparing measured STS images of freestanding InAs quantum dots with those calculated by the full configuration interaction method, we explain the wave function sequence in terms of images of one- and two-electron states. The STS map corresponding to double charging is significantly distorted by electron correlation with respect to the non-interacting case.

PACS numbers: 73.21.La, 73.23.Hk, 73.20.Qt, 31.25.-v

Keywords: quantum dot; Coulomb blockade; scanning tunneling spectroscopy; electron correlation; full configuration interaction

I. INTRODUCTION

Scanning tunneling microscopy (STM) and spectroscopy (STS) is a key tool in nanoscience, allowing for both manipulation of nano-objects and access to their energy spectrum and wave function (WF). The class of systems under study is broad and loosely defined, ranging from nanotubes to quantum dots (QDs) and molecules. Their common features are the possibility of achieving relatively good electrical insulation, the discreteness of their energy spectrum, and the manifestation of Coulomb blockade phenomena at low temperatures. In these few-body systems electron-electron interaction may play a major role, as it is immediately apparent e.g. from single-electron charging experiments.¹

Some of us recently suggested that the WF imaging technique of STS could be a sensitive and direct probe of electron correlation.^{2,3,4,5} Despite recent experimental evidence that few-body semiconductor QDs are strongly affected by electron correlation, as seen both in inelastic light scattering⁶ and high source-drain⁷ spectroscopies, all QD WF images obtained so far, both in real^{8,9,10} and reciprocal^{11,12,13,14} space, were basically interpreted in terms of independent-electron WFs. In this paper we apply many-body tunneling theory to a realistic model which fully takes into account the combined effect of dot anisotropy and Coulomb interaction and predict that STS maps can be strongly distorted by correlation effects. These calculations are validated by a recent low-temperature-STs experiment performed by a few of us on few-electron InAs QDs at the University of Hamburg, which was reported in Ref. 4 and that we here review providing further details and discussion of the theoretical model.

While in this paper we focus exclusively on semicon-

ductor QDs, we stress that the main ideas regarding how electron correlation affects STS could in principle be applied also to short carbon nanotubes as well as single molecules.

The plan of the paper is as follows: After a review of conceptual frameworks used to understand STS (Sec. II), we illustrate our full configuration interaction (FCI) method of calculation of STS images (Sec. III) and theoretically focus on the double charging of a QD in various realistic regimes (Sec. IV). We discuss the evidence of correlation effects provided by the Hamburg experiment (Sec. V), and eventually reconsider our findings in the Conclusions (Sec. VI).

II. THEORY OF THE STS IN THE PRESENCE OF ELECTRON CORRELATION

In order to understand the origin of correlation effects in STS, it is useful to critically reconsider the basic picture of STS performed in the presence of Coulomb blockade. Figure 1 displays schematically the typical energy landscape along the tunneling direction seen by an electron flowing from the STM tip to a drain lead (backgate in Fig. 1) through the QD. The QD is well isolated from tip and backgate by two tunneling barriers (the vacuum and an insulating layer, respectively), so the width of its discrete energy levels is negligible. At low temperature transport occurs mainly due to resonant tunneling through the QD chemical potentials $\mu(N) = E_0(N) - E_0(N-1)$, which are depicted as segments in the QD region of Fig. 1 [N is the number of electrons filling in the QD at equilibrium and $E_0(N)$ is its ground-state energy].¹⁵ If the tip-backgate voltage V is small, current may flow or not (Coulomb blockade) de-

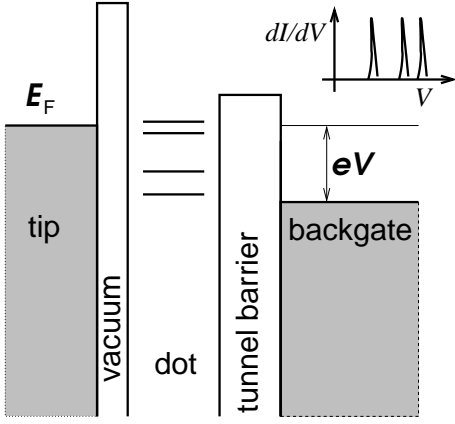


FIG. 1: Simplified energy landscape along the direction of tunneling through a quantum dot for a typical scanning tunneling spectroscopy measurement. E_F is the Fermi energy of the STM tip. Upper right inset: Corresponding idealized dI/dV vs. V plot (ignoring all broadening mechanisms but resonant tunneling).

pending if some value of N exists such that $\mu(N)$ enters the transport energy window. By increasing V one is able to widen the transport window, causing a step in the current I to occur (a peak in the differential conductance dI/dV in the inset of Fig. 1) each time the chemical potential $\mu(N')$ for a new electron number N' enters the window.

In the standard STS mean-field theory,¹⁶ the chemical potentials $\mu(N)$'s are simply Hartree-Fock or Kohn-Sham single-particle (SP) self-consistent levels, split in energy by Coulomb and exchange interactions in addition to the effect of quantum confinement. The energy- and space-resolved local density of SP states, $n(\epsilon, \mathbf{r})$, is just given by a sum over the occupied SP orbitals $\psi_\alpha(\mathbf{r})$, $n(\epsilon, \mathbf{r}) = \sum_\alpha |\psi_\alpha(\mathbf{r})|^2 \delta(\epsilon - \epsilon_\alpha)$, where ϵ_α is the energy of the α th SP level. A general result of many-body time-dependent perturbation theory, valid to first order in the tunneling matrix element,¹⁷ is that dI/dV is proportional to the local electron density. Therefore, in the framework of mean-field theory, the local value of the differential conductance, $dI/dV(E_F, \mathbf{r})$, is given by a sum over the square moduli of SP orbitals whose energies fall in the transport window $\delta\epsilon$ around the Fermi energy E_F , $dI/dV(E_F, \mathbf{r}) \propto \sum_{\delta\epsilon} |\psi_\alpha(\mathbf{r})|^2$. If the energy resolution is sufficient, the space-resolved map of $dI/dV(E_F, \mathbf{r})$ provides the image of the square modulus of a *single* SP orbital, namely the highest-energy occupied QD orbital, akin to the HOMO in molecules. Besides, the STS energy-scan mode exhausts the *Aufbau* filling sequence of the lowest-energy SP levels of the dot.

Since in general the QD energy spectrum strongly depends on electron-electron interaction and consequently on N ,¹⁸ the above mean-field theory suffers a few serious drawbacks: (i) Each tunneling event involves the transition between QD ground states with N and $N + 1$ electrons, therefore it is unclear which value of N should be

used in the N -dependent computation of self-consistent SP orbitals ψ_α .¹⁹ (ii) The interacting N -electron ground state $|\Psi_N\rangle$ is in general a linear superposition of many electronic configurations (Slater determinants), $|\Phi_i^N\rangle$, with expansion coefficients c_i^N , $|\Psi_N\rangle = \sum_i c_i^N |\Phi_i^N\rangle$, while mean-field theory approximates $|\Psi_N\rangle$ with a single Slater determinant, $|\Phi_1^N\rangle$ ($c_i^N = \delta_{i1}$): this approximation turns out to be poor in strongly correlated regimes.²⁰

In order to circumvent the above difficulties we recall from many-body tunneling theory that the differential conductance is proportional to the *interacting* local density of states,²¹

$$dI/dV(E_F, \mathbf{r}) \propto -\frac{1}{\hbar\pi} \text{Im}\mathcal{G}(\mathbf{r}, \mathbf{r}; E_F), \quad (1)$$

where $\mathcal{G}(\mathbf{r}, \mathbf{r}; E_F)$ is the energy- and space-resolved exact zero-temperature retarded Green's function (or one-electron propagator).²² The quantity on the r.h.s. of Eq. (1) (also known as spectral density) may be regarded as the squared modulus of a *quasi-particle* WF:²

$$|\varphi_{\text{QD}}(\mathbf{r})|^2 = -\frac{1}{\hbar\pi} \text{Im}\mathcal{G}(\mathbf{r}, \mathbf{r}; E_F). \quad (2)$$

The quasi-particle WF $\varphi_{\text{QD}}(\mathbf{r})$ is the natural generalization of the SP WF to strongly correlated regimes. In the non-interacting limit $\varphi_{\text{QD}}(\mathbf{r}) \rightarrow \psi(\mathbf{r})$, as we show below. In practice, the calculation of $\varphi_{\text{QD}}(\mathbf{r})$ requires the knowledge of the (configuration interaction) expansion coefficients c_j^N and c_i^{N-1} of the interacting ground-states $|\Psi_N\rangle$ and $|\Psi_{N-1}\rangle$ with both N and $N - 1$ electrons, respectively, according to the formula $\varphi_{\text{QD}}(\mathbf{r}) = \sum_{i,j} c_i^{N-1} c_j^N \psi_{\alpha(i,j)}(\mathbf{r})$, where $\alpha(i,j)$ is a SP quantum index depending on both Slater determinants $|\Phi_i^{N-1}\rangle$ and $|\Phi_j^N\rangle$. Distortion effects of $\varphi_{\text{QD}}(\mathbf{r})$ with respect to $\psi(\mathbf{r})$ are due to the quantum interference among different SP orbitals $\psi_{\alpha(i,j)}(\mathbf{r})$. In the non-interacting limit, both N - and $(N - 1)$ -electron ground states are single Slater determinants, $c_i^{N-1} = \delta_{i1}$, $c_j^N = \delta_{j1}$, and therefore $\varphi_{\text{QD}}(\mathbf{r})$ reduces to the simple SP orbital $\psi_{\alpha(1,1)}(\mathbf{r})$.

III. PREDICTING STS MAPS FROM FULL CONFIGURATION INTERACTION

We consider a two-dimensional QD with parabolic lateral confinement, which is a commonly accepted approximation¹⁸ in the framework of the envelope-function description of SP states:

$$H_0(i) = \frac{\mathbf{p}_i^2}{2m^*} + \frac{1}{2}m^*(\omega_x^2 x_i^2 + \omega_y^2 y_i^2). \quad (3)$$

In the SP Hamiltonian for the i th electron of Eq. (3) the lateral confinement is different in the x and y directions (with corresponding confinement frequencies ω_x and ω_y , respectively): Such an elliptical confinement mimics the combined effects of geometrical deviations from perfect circularity and/or atomistic effects²³ due to strain,

piezoelectric fields, interface matching, which lower the symmetry point-group from $D_{\infty h}$ (circular case) to C_{2v} [the symmetry point-group of the Hamiltonian (3), D_{2h} , is actually slightly larger than the C_{2v} group]. In addition, we include into our model the full Coulomb interaction among the N electrons populating the dot:

$$H = \sum_i^N H_0(i) + \frac{1}{2} \sum_{i \neq j} \frac{e^2}{\kappa |\mathbf{r}_i - \mathbf{r}_j|}. \quad (4)$$

In Eqs. (3-4) e and κ are respectively the electron charge and static relative dielectric constant of the host semiconductor, \mathbf{p} is the canonically conjugated momentum of position $\mathbf{r} \equiv (x, y)$, m^* is the electron effective mass.

We solve numerically the few-body problem of Eq. (4) for the ground states of N and $N - 1$ electrons by means of the FCI method, that we successfully applied in predicting QD transport²⁴ and Raman⁶ spectra (for full details on our FCI method, its performances, and ranges of applicability, see Ref. 20). Briefly, we expand the N -electron interacting ground state $|\Psi_N\rangle$ on the basis of the Slater determinants $|\Phi_i^N\rangle$ obtained by filling in with N electrons in all possible ways a subset of the SP orbitals, eigenstates of Hamiltonian (3). On the Slater-determinant basis, the Hamiltonian (4) is a large, sparse matrix that we diagonalize by means of a parallel state-of-the-art Lanczos code. The expansion coefficients c_i^N , which are the output of the FCI calculation, are eventually used to build the quasi-particle WF $\varphi_{\text{QD}}(\mathbf{r})$.

IV. QUASI-PARTICLE IMAGES IN REALISTIC QUANTUM DOTS: THEORY

We here consider quasi-particle WF images for realistic QDs predicted by the theory of Secs. II-III, focusing on the simplest case where electron correlation becomes relevant, namely the tunneling transition $N = 1 \rightarrow N = 2$. In fact, the image of the first charging process $N = 0 \rightarrow N = 1$ is simply given by the lowest-energy SP orbital.

We first investigate the case of a circular QD by monitoring the evolution of the square modulus of $\varphi_{\text{QD}}(\mathbf{r})$ as a function of the lateral confinement energy $\hbar\omega_0 = \hbar\omega_x = \hbar\omega_y$. On a general basis, we expect that correlation effects are negligible in the non-interacting limit $\hbar\omega_0 \rightarrow \infty$ while they dominate in the opposite limit $\hbar\omega_0 \rightarrow 0$. In fact, the SP [Eq. (3)] and the Coulomb [Eq. (4)] terms of the interacting Hamiltonian scale differently with $\hbar\omega_0$, the former as $\sim \hbar\omega_0$ and the latter as $\sim \sqrt{\hbar\omega_0}$ (Ref. 2). When $\hbar\omega_0 \rightarrow \infty$ the SP term dominates with respect to the Coulomb term, and the ground state is essentially a single Slater determinant, while interaction effects can be regarded as a perturbation: in this limit mean-field theory is expected to give correct predictions. In the opposite limit, instead, the Coulomb term very effectively mixes many Slater determinants, and significant distortions of $\varphi_{\text{QD}}(\mathbf{r})$ with respect to the non-interacting case are expected.

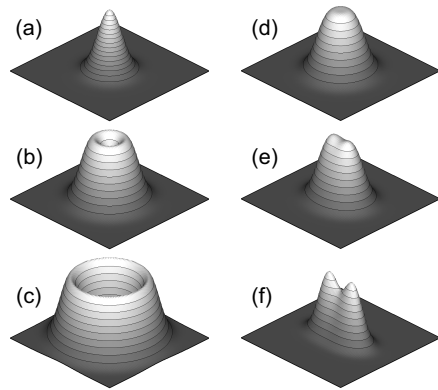


FIG. 2: Calculated STS maps for the ground state \rightarrow ground state transition $N = 1 \rightarrow N = 2$, as a function of lateral confinement energy $\hbar\omega_0$ and dot anisotropy. (a-c) Dependence of the STS image on the lateral confinement energy $\hbar\omega_0$ in the case of a circular dot. Plots (a-c) correspond to $\hbar\omega_0 = +\infty$, 0.5, 0.01 meV, respectively, with $\omega_0 = \omega_x = \omega_y$. (d-e) Dependence of the STS image on the dot anisotropy. Plots (d-e) correspond to $\omega_x/\omega_y = 1, 1.1, 1.5$, respectively, with $\hbar\omega_y = 2$ meV. The lateral extension of all plots is 4×4 units of the characteristic lateral extension of the harmonic oscillator $\ell_{\text{QD}} = [\hbar/(m^*\omega_y)]^{1/2}$, and GaAs parameter are used throughout the paper. Plot heights are renormalized arbitrarily. The absolute norms of STS maps are given in Table I.

Figures 2(a-c) display the maps of $|\varphi_{\text{QD}}(\mathbf{r})|^2$ in the (x, y) plane for decreasing values of $\hbar\omega_0$ [from top to bottom, $\hbar\omega_0 \rightarrow +\infty$ (a), $\hbar\omega_0 = 0.5$ meV (b), $\hbar\omega_0 = 0.01$ meV (c)]. In the non-interacting case [Fig. 2(a)], the STS map is just a replica of the SP $1s$ orbital, eigenstate of the 2D harmonic oscillator (a 2D gaussian), corresponding to the injection of a second electron into the same $1s$ level occupied by the first electron with opposite spin, according to Pauli exclusion principle. As $\hbar\omega_0$ is decreased, we see that a significant portion of weight is moved from the image center into an outer ring [Fig. 2(b)]. In a very shallow dot [Fig. 2(c)], the dot center is completely emptied and the STS image now looks like a donut. The latter case of strong interaction shows that the STS image can be very different from that expected by a naive application of the Aufbau principle, due to the hybridization of higher-energy SP orbitals with the $1s$ WF.

In Fig. 2 the length unit is the characteristic lateral extension of the harmonic oscillator, $\ell_{\text{QD}} = [\hbar/(m^*\omega_y)]^{1/2}$, which depends on $\hbar\omega_y$, and $\varphi_{\text{QD}}(\mathbf{r})$ is arbitrarily normalized. Another effect of correlation is the loss of absolute weight of the quasi-particle WF as $\hbar\omega_0$ is decreased.² Table I shows the norm of $\varphi_{\text{QD}}(\mathbf{r})$ for the cases displayed in Fig. 2. We see that the reduction of the confinement energy $\hbar\omega_0$ in a circular QD is associated to a dramatic weight loss. This trend may be seen as a signature of the Wigner crystallization of the $(N - 1)$ - and N -electron ground states which manifests itself as

TABLE I: Norm of the quasi-particle, $\int d\mathbf{r} |\varphi_{\text{QD}}(\mathbf{r})|^2$, for different ground-state \rightarrow ground-state tunneling transitions $N = 1 \rightarrow N = 2$. The weight ranges between 0 and 1.

Case ^a	Quasi-particle weight	Case	Quasi-particle weight
(a)	1.00	(d)	0.794
(b)	0.633	(e)	0.793
(c)	0.109	(f)	0.720

^aThe case refers to the calculated STS image displayed in Fig. 2.

an increased “rigidity” of the states opposing electron injection.

We now switch to consider the effect of dot anisotropy, since the dependence of STS images on dot ellipticity was found to be a major issue in the Hamburg experiment (cf. Sec. V below).⁴ In Fig. 2(d) we start showing the predicted STS map for a circular QD with $\hbar\omega_0 = 2$ meV, and then modify its ellipticity by increasing the lateral frequency ratio ω_x/ω_y , going from $\omega_x/\omega_y = 1.1$ [Fig. 2(e)] up to $\omega_x/\omega_y = 1.5$ [Fig. 2(f)]. By doing so, as we move downwards in the right column of Fig. 2, we expect to “squeeze” the quasi-particle WF along the x direction, which is indeed observed for both single and double charging processes. However, in the present double charging case, we also see an unexpected effect, i.e. the quasi-particle WF develops two peaks along the y -axis. This surprising distortion is due to the destructive interference between $1s$ and $1d$ states of the harmonic oscillator along y (belonging to the same representation A of the D_{2h} group), which is a correlation effect. This can also be seen as a manifestation of the general statement that the importance of correlation increases as the system dimensionality is reduced (from 2D to 1D).

To conclude this section, we mention that another issue relevant to STS images is the type of dielectric environment felt by QD electrons.⁴ Specifically, the dielectric mismatch between vacuum and InAs in the Hamburg experiment affects both the SP confinement potential (self-polarization effect) and the electron-electron interaction (interaction with surface image charges of like sign), therefore changing the relative importance of their effect on the ground state. Qualitatively, we expect that changing the dielectric environment causes effects similar to those obtained by modifying $\hbar\omega_0$.

V. STS IMAGING OF FEW-ELECTRON MBE-GROWN QUANTUM DOTS: EXPERIMENT

We studied strain-induced InAs QDs grown on n-doped GaAs(001) substrates by molecular beam epitaxy (MBE).¹⁰ An undoped tunneling barrier 5 nm thick insulates the freestanding QDs from a n-doped GaAs buffer layer 200 nm thick, acting as a backgate for the current flowing from the STM tip through the QDs. The samples were transferred from the MBE into the STM chamber

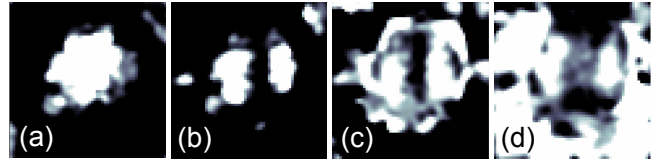


FIG. 3: $dI/dV(E, \mathbf{r})$ spatial maps recorded at the voltages 840 (map a), 1040 (b), 1140 (c), and 1350 (d) mV, respectively, for a representative QD. The size of all maps is 30×30 nm. White (black) colour stands for high (low) values of dI/dV . $I_{\text{stab}} = 100$ pA, $V_{\text{stab}} = 1500$ mV, $V_{\text{mod}} = 4$ mV.

in ultra-high vacuum without being exposed to the air by means of a mobile system, in order to avoid contamination, and STM was operated at a background pressure smaller than 10^{-10} mbar and at $T = 6$ K with maximum energy resolution of $\delta\varepsilon = 2$ meV.²⁵ STM images were taken in constant-current mode, with a typical sample bias in the range of 2-4 V and a tunneling current of 20-40 pA. A lock-in technique (modulation voltage V_{mod} in the range of 5-20 mV) was used to record $dI/dV(E, \mathbf{r})$ and WF mapping was carried out over a specified area by stabilizing the tip-surface distance in each point \mathbf{r} at voltage V_{stab} and current I_{stab} , switching off the feedback and recording a dI/dV curve from V_{start} to V_{end} ($V_{\text{start}} \leq V_{\text{stab}}$).¹⁰ As a result, WF mapping produces a 3D array of dI/dV data, which allows obtaining spatially resolved $dI/dV(E, \mathbf{r})$ images at different values of sample voltages.

In Fig. 3 we show $dI/dV(E, \mathbf{r})$ maps of a representative QD measured at fixed voltages corresponding to four clearly localized QD WFs, labeled (a), (b), (c), and (d), respectively, in order of increasing energy.⁴ We observed a pronounced shape anisotropy for all dots, which have a pyramidal shape with well-defined facets, consistently with previous findings.^{10,26} This is evident also from the elongation of images (b), (c), and (d) of Fig. 3 along the $[1\bar{1}0]$ direction. In detail, WF maps of Fig. 3 show the following approximate symmetries, going from low to high-energy: s -like for (a), p -like for (b) and (c), and possibly (d). The (d) image is somehow blurred, likely because states of the wetting layer overlapping in energy with (d) significantly contribute to the spectral density. See Ref. 4 for further discussion.

As expected for the square moduli of the two lowest-energy SP $1s$ and $2p$ orbitals, images (a) and (b) exhibit a roughly circular symmetric intensity distribution and elongation along the $[1\bar{1}0]$ direction with a node in the center, respectively (Fig. 3). Unexpectedly, image (c) shows again a p -like symmetry in the $[1\bar{1}0]$ direction, as before, instead of $[110]$ as expected for the second $2p$ orbital.¹⁰ As a consequence, it is not possible to explain the WF sequence [and map (c) in particular] in terms of SP orbitals, since in this case we would expect the appearance of either a single $2p$ or two $2p$ states elongated in the $[1\bar{1}0]$ and $[110]$ directions, respectively. On the other hand, from a mean-field point of view the charge

ing of the same $2p$ orbital with a second electron can be excluded since a replica is not observed for the $1s$ orbital.

On this basis, we believe that the understanding of the data of Fig. 3 must rely on the theory developed in Sec. IV, taking into account the combined effect of electron correlation, dot anisotropy, and dielectric mismatch. Specifically, we assign maps (a) and (b) to the tunneling events $N = 0 \rightarrow N = 1$ corresponding to resonances through $1s$ and $2p$ SP states, while we associate image (c) of Fig. 3 to the ground state \rightarrow ground state charging process $N = 1 \rightarrow N = 2$, showing features similar to those predicted in Figs. 2(e-f). Further support for this interpretation is reported in Ref. 4.

VI. CONCLUSIONS

In this paper we have focused on QDs where electron-electron interaction may be relevant, showing that the STS technique is sensitive to quasi-particle WFs and that their images can be greatly affected by electron corre-

lation. On the basis of FCI calculations of STS maps which fully take into account correlation effects and dot anisotropy, we have been able to understand measured WF images of freestanding self-assembled InAs quantum dots. We identified ground- and excited-state WFs corresponding to the injection of a first and a second electron into the QD. Correlation effects are found to distort the WF corresponding to double charging in an essential way. We believe our findings may be relevant to a broader class of experiments, including STS on carbon nanotubes and single molecules.

Acknowledgments

This work is supported by the INFM-CINECA Supercomputing Project 2006, the MIUR-FIRB Project RBIN04EY74, the EU-network project Nanospectra, and the Deutsche Forschungsgemeinschaft (SFB508, TP A6 and B7).

-
- * Electronic address: rontani@unimore.it; URL: http://www.nanoscience.unimo.it/max_index.html
- † Permanent address: CNR-INFM National Research Center NNL, Distretto Tecnologico ISUFI Via Arnesano, 73100 Lecce, Italy; Electronic address: giuseppe.maruccio@unile.it
- ¹ H. Grabert and M. H. Devoret, *Single charge tunneling: Coulomb blockade phenomena in nanostructures*, vol. 294 of *NATO ASI series B: physics* (Plenum, New York, 1992).
 - ² M. Rontani and E. Molinari, Phys. Rev. B **71**, 233106 (2005).
 - ³ M. Rontani and E. Molinari, Jpn. J. Appl. Phys. **45**, 1966 (2006).
 - ⁴ G. Maruccio, M. Janson, A. Schramm, C. Meyer, T. Matsui, C. Heyn, W. Hansen, R. Wiesendanger, M. Rontani, and E. Molinari, Nano Letters **7** (2007), in press, available on the web (DOI:10.1021/nl071133m) and as arXiv:0707.4613v1.
 - ⁵ M. Rontani, Int. J. Mod. Phys. B **20**, 5311 (2006), also available as cond-mat/0602263.
 - ⁶ C. P. García, V. Pellegrini, A. Pinczuk, M. Rontani, G. Goldoni, E. Molinari, B. S. Dennis, L. N. Pfeiffer, and K. W. West, Phys. Rev. Lett. **95**, 266806 (2005).
 - ⁷ M. Korkusiński, P. Hawrylak, M. Ciorga, M. Pioro-Ladrière, and A. S. Sachrajda, Phys. Rev. Lett. **93**, 206806 (2004).
 - ⁸ B. Glandier, Y. M. Niquet, B. Legrand, J. P. Nys, C. Priester, D. Stiévenard, J. M. Gérard, and V. Thierry-Mieg, Phys. Rev. Lett. **85**, 1068 (2000).
 - ⁹ O. Millo, D. Katz, Y. W. Cao, and U. Banin, Phys. Rev. Lett. **86**, 5751 (2001).
 - ¹⁰ T. Maltezopoulos, A. Bolz, C. Meyer, C. Heyn, W. Hansen, M. Morgenstern, and R. Wiesendanger, Phys. Rev. Lett. **91**, 196804 (2003).
 - ¹¹ E. E. Vdovin, A. Levin, A. Patanè, L. Eaves, P. C. Main, Y. N. Khanin, Y. V. Dubrovskii, M. Henini, and G. Hill, Science **290**, 122 (2000).
 - ¹² A. Patanè, R. J. A. Hill, L. Eaves, P. C. Main, M. Henini, M. L. Zambrano, A. Levin, N. Mori, C. Hamaguchi, Y. V. Dubrovskii, et al., Phys. Rev. B **65**, 165308 (2002).
 - ¹³ O. S. Wibbelhoff, A. Lorke, D. Reuter, and A. D. Wieck, Appl. Phys. Lett. **86**, 092104 (2005).
 - ¹⁴ P. Kailuweit, D. Reuter, A. D. Wieck, O. S. Wibbelhoff, A. Lorke, U. Zeitler, and J. C. Maan, Physica E **32**, 159 (2006).
 - ¹⁵ For the sake of simplicity, we here ignore contribution of excited states to transport as well as higher-order and non-equilibrium effects.
 - ¹⁶ J. Tersoff and D. R. Hamann, Phys. Rev. B **31**, 805 (1985).
 - ¹⁷ J. Bardeen, Phys. Rev. Lett. **6**, 57 (1961).
 - ¹⁸ S. M. Reimann and M. Manninen, Rev. Mod. Phys. **74**, 1283 (2002).
 - ¹⁹ Note that the question is irrelevant for extended systems where self-consistent SP orbitals do not depend significantly on N .
 - ²⁰ M. Rontani, C. Cavazzoni, D. Bellucci, and G. Goldoni, J. Chem. Phys. **124**, 124102 (2006).
 - ²¹ T. E. Feuchtwang, Phys. Rev. B **10**, 4121 (1974).
 - ²² M. Rontani, Phys. Rev. Lett. **97**, 076801 (2006).
 - ²³ G. Bester and A. Zunger, Phys. Rev. B **71**, 045318 (2005).
 - ²⁴ T. Ota, M. Rontani, S. Tarucha, Y. Nakata, H. Z. Song, T. Miyazawa, T. Usuki, M. Takatsu, and N. Yokoyama, Phys. Rev. Lett. **95**, 236801 (2005).
 - ²⁵ C. Wittneven, R. Dombrowski, S. H. Pan, and R. Wiesendanger, Rev. Sci. Instrum. **68**, 3806 (1997).
 - ²⁶ J. Márquez, L. Geelhaar, and K. Jacobi, Appl. Phys. Lett. **78**, 2309 (2001).